



**HAL**  
open science

## **Polydopamine treatment of chitosan nanofibers for the conception of osteoinductive scaffolds for bone reconstruction**

Syrine Dimassi, Nicolas Tabary, Feng Chai, Cedric Zobrist, Jean-Christophe Hornez, Frederic Cazaux, Nicolas Blanchemain, Bernard Martel

### ► To cite this version:

Syrine Dimassi, Nicolas Tabary, Feng Chai, Cedric Zobrist, Jean-Christophe Hornez, et al.. Polydopamine treatment of chitosan nanofibers for the conception of osteoinductive scaffolds for bone reconstruction. Carbohydrate Polymers, 2022, Carbohydrate Polymers, 276, pp.118774. 10.1016/j.carbpol.2021.118774 . hal-03405054

**HAL Id: hal-03405054**

**<https://hal.univ-lille.fr/hal-03405054>**

Submitted on 5 Jan 2024

**HAL** is a multi-disciplinary open access archive for the deposit and dissemination of scientific research documents, whether they are published or not. The documents may come from teaching and research institutions in France or abroad, or from public or private research centers.

L'archive ouverte pluridisciplinaire **HAL**, est destinée au dépôt et à la diffusion de documents scientifiques de niveau recherche, publiés ou non, émanant des établissements d'enseignement et de recherche français ou étrangers, des laboratoires publics ou privés.



Distributed under a Creative Commons Attribution - NonCommercial 4.0 International License

# 1           **Polydopamine treatment of chitosan nanofibers for the conception of** 2                           **osteoinductive scaffolds for bone reconstruction**

3   Syrine Dimassi<sup>a</sup>, Nicolas Tabary<sup>a</sup>, Feng Chai<sup>b</sup>, Cédric Zobrist<sup>a</sup>, Jean-Christophe Hornez<sup>c</sup>, Frédéric  
4   Cazaux<sup>a</sup>, Nicolas Blanchemain<sup>b</sup> and Bernard Martel<sup>a\*</sup>

5   <sup>a</sup> Univ. Lille, CNRS, INRA, ENSCL UMR8207, UMET – Unité Matériaux et Transformations, Lille, France

6   <sup>b</sup> Univ. Lille, INSERM, CHU Lille, U1008 – Controlled Drug Delivery Systems and Biomaterials, Lille, France

7   <sup>c</sup> Université Polytechnique Hauts de France, LMCPA, Maubeuge, France

8

9   \*Corresponding authors:

10   Bernard Martel; E-mail address: [bernard.martel@univ-lille.fr](mailto:bernard.martel@univ-lille.fr)

11

## 12   **Abstract**

13   We report the influence of treatment time of electrospun chitosan nanofibers (CHT NFs) in dopamine  
14   hydrochloride bath (2 mg. mL<sup>-1</sup> in 10 mM Tris buffer, pH 8.5) on the extent of the polydopamine  
15   (pDA) coating on NFs surface. The reaction was characterized by FTIR and SEM analysis and the  
16   cytocompatibility of the scaffolds toward MT3C3-E1 cells was assessed. Biomimetic deposition of  
17   hydroxyapatite (HA) in 1.5xSBF batch was investigated by SEM-EDS and XRD. Samples treated in  
18   dopamine bath during 2 h promoted the structural stability of NFs in PBS, provided optimal  
19   cytocompatibility and induced the in vitro biomineralization from 6 days in 1.5xSBF. The XRD and  
20   SEM-EDS investigations confirmed formation of spherical-shaped particles composed of apatitic  
21   phase. Finally, this study shows that these NFs-pDA scaffolds prepared in the optimal experimental  
22   conditions defined here are promising candidates for application as osteoinductive scaffolds for bone  
23   regeneration applied to orthopaedic and dental applications

24

25    *Keywords: electrospinning; nanofibers; polydopamine; scaffolds; hydroxyapatite; bone tissue*  
26    *engineering*

27

## 28   **1. Introduction**

29   Bone tissue engineering (BTE) has been discovered in the 1990s and its interest has grown  
30   exponentially over the years. It holds a great promise for the treatment of bone diseases or defects  
31   (Ranganathan, Balagangadharan & Selvamurugan, 2019). One of the main components of BTE is the  
32   scaffold that should mimic the extracellular matrix (ECM) and provide a three-dimensional  
33   environment for cells and biological molecules to grow and regenerate tissue (Ehrbar, Lütolf, Rizzi,  
34   Hubbell & Weber, 2008). Thus, 3D-scaffold should have a highly porous structure with interconnected

35 pores and an extremely large specific surface area (Liu, Cui, Zhuang, Wei & Chen, 2014). Various  
36 methods for fabrication of porous scaffolds that mimics the natural ECM are developed, such as phase  
37 separation (Ciapetti et al., 2012; Salerno, Fernández-Gutiérrez, San Román del Barrio & Domingo,  
38 2015), freeze-drying (Chong, Zarith & Sultana, 2015; Flores et al., 2016; Shahbazarab, Teimouri,  
39 Chermahini & Azadi, 2018) , auto-assembly (Nie, Li, Lu, Lei, Zhang & Wang, 2013; Pan, Chen,  
40 Metavarayuth, Su & Wang, 2018) and electrospinning (Chen et al., 2017; Jang, Castano & Kim, 2009;  
41 Liao, Murugan, Chan & Ramakrishna, 2008; Sharifi, Atyabi, Norouzian, Zandi, Irani & Bakhshi,  
42 2018).

43 Electrospinning, a relatively simple and useful fabrication technique, is extensively used to  
44 manufacture nonwoven mats of fibers with diameters ranging from several microns down to less than  
45 100 nm (Chen, Li, Li & Xie, 2018; Wen, Zong, Linhardt, Feng & Wu, 2017). The intrinsic properties  
46 of resulted scaffolds offer a familiar environment to cells promoting their adhesion and proliferation.  
47 Further, it is possible to modulate nanofibers morphology, as the size of fibers diameters and the  
48 pores, by optimizing solution, process and/ or environmental parameters, and properties of scaffolds  
49 depending on biomaterial choice (Gupta, Haider, Choi & Kang, 2014; Haider, Haider & Kang, 2018;  
50 Kwak, Haider, Gupta, Kim & Kang, 2016)

51 Chitosan (CHT), a linear polysaccharide naturally present in fungi or obtained from deacetylation of  
52 chitin and made up of D-glucosamine and N-acetyl-D-glucosamine repeating units linked through  $\beta$   
53 (1,4)- linkages, has emerged as a promising candidate for bone tissue engineering. Indeed, CHT has a  
54 similar structure to that of bone extracellular glycosaminoglycan and thus presents various properties  
55 such as biocompatibility, non-toxicity, biodegradability, etc. (Balagangadharan, Dhivya &  
56 Selvamurugan, 2017; LogithKumar, KeshavNarayan, Dhivya, Chawla, Saravanan & Selvamurugan,  
57 2016). Studies have reported that CHT plays an important role in the enhancement of cell adhesion  
58 and proliferation, osteoblast differentiation and mineralization (Balagangadharan, Dhivya &  
59 Selvamurugan, 2017; LogithKumar, KeshavNarayan, Dhivya, Chawla, Saravanan & Selvamurugan,  
60 2016; Pattnaik, Nethala, Tripathi, Saravanan, Moorthi & Selvamurugan, 2011; Sainitya et al., 2015;  
61 Saravanan, Nethala, Pattnaik, Tripathi, Moorthi & Selvamurugan, 2011). Nevertheless, CHT needs to  
62 be associated with other polymers (natural or synthetic ones), metals and/or ceramics in order to  
63 promote its properties as mechanical strength and structural integrity for BTE applications. First of all,  
64 for processing CHT by electrospinning, it has to be mixed with a non-ionic polymer such as  
65 polyethyleneoxide (PEO) for promoting chains entanglements and thus facilitate electrospinning  
66 process (Frohbergh et al., 2012; Jiang, Deng, James, Nair & Laurencin, 2014; Khajavi, Abbasipour &  
67 Bahador, 2016; Levengood & Zhang, 2014; Norowski Jr et al., 2015; Shalumon, Sowmya, Sathish,  
68 Chennazhi, Nair & Jayakumar, 2013; Van Hong Thien, Hsiao, Ho, Li & Shih, 2013; Yang, Chen &  
69 Wang, 2009). In addition, if CHT nanofibers provide the structural properties for BTE applications, it

70 does not intrinsically present osteoinductive properties. Therefore, chitosan nanofibers are often  
71 chemically modified after their spinning, or used in combination with other materials that provide the  
72 biochemical cues for acceleration of bone regeneration. (Balagangadharan, Dhivya & Selvamurugan,  
73 2017).

74 Globally, functionalization of biomaterials promoting the pre-osteoblast cells proliferation and  
75 mineralization process has been extensively studied in literature, (Bose, Robertson & Bandyopadhyay,  
76 2018; Hu, Ashok, Nisbet & Gautam, 2019; Jiao & Cui, 2007). Biomineralization is a regulated process  
77 by which living organisms produce mineral phase composed of calcium phosphate, which is an  
78 essential requirement for the normal skeletal development of bone tissue. Therefore, studies have been  
79 conducted to promote the growth of apatitic phase (most commonly hydroxyapatite) at the surface and  
80 within the bone matrix. This would promote adhesion, proliferation and differentiation of bone cells,  
81 and thus stimulate bone formation and regeneration of natural bone tissue. Therefore, many  
82 investigations have reported the use of a simple, effective and bio-inspired strategy that consists of the  
83 functionalization of biomaterials with polydopamine (pDA), that has generated a great interest in  
84 several areas of nanomedicine, from biosensors to tissue engineering (Ho & Ding, 2014; Lee *et al.*,  
85 2016; Lynge, van der Westen, Postma & Städler, 2011; Tsai, Chen, Chien, Kuo & Wang, 2013). Ko *et al.*  
86 studied the grafting of peptides derived from bone morphogenetic factor 2 (BMP-2) on PLGA films  
87 functionalized with pDA. They demonstrated the ability of these materials to regulate osteogenic  
88 differentiation and *in vitro* and *in vivo* mineralization of human adipose stem cells (hADSC) (Ko,  
89 Yang, Shin & Cho, 2013). Similarly, Cho *et al.* have described the immobilization of BMP-2 growth  
90 factors on the surface of PCL nanoparticles coated with pDA to improve bone regeneration *in vivo*  
91 (Cho *et al.*, 2014). Kwon *et al.* treated polyetheretherketone (PEEK) surface with pDA for the covalent  
92 immobilization of collagen or insulin. They report that this treatment increased the bioactivity of the  
93 PEEK surface allowing for adhesion, proliferation and osteogenic differentiation of MC3T3-E1 cells  
94 which could enhance tissue integration of biomedical implants (Kwon, Kim, Gupta & Kang, 2018).

95 Ryu *et al.* have introduced a universal biomineralization pathway capable of forming hydroxyapatite  
96 crystals on the surface of various materials, including ceramics, noble metals, semiconductors and  
97 synthetic polymers. They showed that catecholamine groups present in pDA were responsible for the  
98 adhesion and nucleation of hydroxyapatite in the presence of Ca<sup>2+</sup> ions at the interface. After  
99 incubation for two weeks in a simulated body fluid (SBF), the functionalized titanium metal implant  
100 was completely and uniformly covered with calcium phosphate (CaP) minerals, unlike virgin  
101 biomaterial (Ryu, Ku, Lee & Park, 2010). Introduced for the first time by Kokubo *et al.* to evaluate the  
102 surface changes of bioactive bioceramics (Kokubo, 1991), it is widely used as an *in vitro*  
103 characterization method to study apatite layer formation on the surface of implants and thus predict  
104 their osteoinductive properties *in vivo* (Chen, Nouri, Li, Lin, Hodgson & Wen, 2008; Kokubo &  
105 Takadama, 2006).

106 In particular, very few papers report the pDA treatment of electrospun materials intended for  
107 biomedical applications. Very recently, Ma et al. (Ma et al., 2021) and Zia et al. (Zia, Tabassum,  
108 Meng, Xin, Gong & Li, 2021) reported the treatment of electrospun substrates with pDA for  
109 promoting the immobilization of chitosan on the NFs forming functional coatings providing anti  
110 bacterial activity and heavy metal ions sorption, respectively. Interestingly, Ziu *et al.* reported the  
111 elaboration of a composite PLLA-CHT interpenetrated fibrous network treated with pDA that  
112 displayed enhanced mechanical properties and osteogenic activity (Liu et al., 2017).

113 If the treatment of nanofibrous electrospun scaffolds by pDA for biomedical (and other) applications  
114 have been already reported in literature, the former studies do not discuss the influence of the  
115 parameters of the pDA treatment step on the subsequent steps for their functionalization neither on  
116 their intrinsic physicochemical nor biological properties. Therefore, in this paper we report in depth  
117 the influence of the time of treatment of CHT NFs in the dopamine solution on the chemical  
118 composition of the NFs, and we aimed to define the optimal compromise between the pDA treatment  
119 time and i) the stability of the NFs in aqueous medium, ii) the cytocompatibility toward pre-  
120 osteoblasts MC3T3-E1 and iii) the capacity to promote the nucleation of hydroxyapatite. The results  
121 obtained showed that the materials obtained in optimized experimental conditions of pDA treatment  
122 display promising properties for use in tissue engineering and especially as scaffolds for bone  
123 reconstruction.

124

125

## 126 **2. Materials and methods**

### 127 **2.1. Materials**

128 Chitosan (CHT), low molecular weight grade batch WA1603121, 98.26% degree of deacetylation, was  
129 supplied by WISapple with a molecular weight of 200 000 g.mol<sup>-1</sup> (supplier values). Polyethylene  
130 oxide (PEO, 900 000 g.mol<sup>-1</sup>), glacial acetic acid, phosphate buffered saline (PBS), dopamine  
131 hydrochloride and Trizma® base (Tris) were purchased from Sigma Aldrich (Saint-Quentin Fallavier,  
132 France).

133 All reagents were used as received from the manufacturer without further purification. Ultrapure water  
134 was used for all experiments (Veolia water aquadem, Purelab flex, ELGA, 18.2 MΩ).

### 135 **2.2. Electrospinning process**

136 CHT/PEO blend solutions were prepared at 3.3 wt % concentration, with a ratio CHT: PEO of 9:1, in  
137 90% (v/v) acetic acid solution. The solution mixing was performed at room temperature with  
138 mechanical stirring of 300 rpm for 12 h to ensure complete dissolution of the solutes to obtain  
139 homogeneous solutions. The spun solution was filled into a 5 mL plastic syringe connected to a  
140 21gauge needle through a polyethylene catheter (inner diameter 1 mm, VYGON) and placed onto a

141 syringe pump (Fisher Scientific). The electrospinning process was carried out at a flow rate of 0.3  
142 mL.h<sup>-1</sup>, a voltage between 12 and 15 kV and a tip-to-collector distance of 20 cm. Relative humidity  
143 and temperature were fixed at 33 ± 2 % and 21 ± 2°C, respectively. Nanofiber mats were collected on  
144 a roll collector (diameter 90 mm, rotation speed 150 rpm) and then thermally post-treated at 140 °C for  
145 4 h under vacuum in order to improve their stability in aqueous medium.

### 146 **2.3. Preparation of NFs pDA**

147 The protocol described by Messersmith *et al.* has been adapted for the treatment of CHT NFs (Lee,  
148 Dellatore, Miller & Messersmith, 2007). We also relied on the work of Ryu *et al.* (Ryu, Ku, Lee &  
149 Park, 2010). The CHT/ PEO blend nanofibrous scaffolds were first cut into square shaped samples (4 x  
150 4 cm) and immersed into dopamine hydrochloride solution (2 mg. mL<sup>-1</sup> in 10 mM Tris buffer, pH 8.5)  
151 at room temperature, under mechanical stirring and at open air conditions to promote dopamine's  
152 oxidation and polymerization. Different times of immersion were studied, ranging from 2 hours up to  
153 5 days and the dopamine solution was renewed every day. Then, polydopamine coated samples (NFs  
154 pDA) were thoroughly rinsed with ultrapure water followed by three washes in an ultrasound bath to  
155 remove the unreacted dopamine and were air-dried for 24 h.

### 156 **2.4. Characterization of functionalized scaffolds**

#### 157 **2.4.1. Scanning Electron Microscopy**

158 The morphological architectures of diverse membranes and scaffolds were observed using scanning  
159 electron microscopy (SEM) (Hitachi S-4700 SEM field emission GU) with an accelerating voltage of  
160 5 kV and an emission current of 10 µA. All specimens were sputtered with a thin layer of chrome  
161 before imaging. Fibres diameter distribution and standard deviation were determined by ImageJ.  
162 Software using SEM images.

#### 163 **2.4.2. FTIR spectroscopy**

164 Scaffolds were investigated by Attenuated Total Reflectance-Fourier Transformed Infrared (ATR-  
165 FTIR) using a PERKINELMER spectrometer (SpectrumOne) equipped with Spectrum software.  
166 Spectra were recorded from 4000 to 650 cm<sup>-1</sup> (Scan number of 16) with a resolution of 4 cm<sup>-1</sup>.

#### 167 **2.4.3. Colorimetric quantification of amino groups**

171  
172 Density of surface amino groups of samples was carried out by performing a colorimetric assay  
173 with the sodium salts of orange II (Orange acid II, AO II, MW 350.32 g.mol<sup>-1</sup>, ≥ 85%, Sigma  
174 Aldrich™). An aqueous solution of AO II at 2.5 × 10<sup>-2</sup> mol.L<sup>-1</sup> was prepared in ultrapure water at pH  
175 3 (adjusted with 0.5 mol.L<sup>-1</sup> of HCl solution. Each sample (disk of 11 mm in diameter) was  
176 impregnated in 10 mL of this solution, under orbital shaking of 70 rpm, at room temperature and  
177 protected from light, at least for 12 h. Samples were then washed three times (5 minutes each) in 20

178 ml of ultrapure water which pH has been adjusted to 3 with a HCl solution at 0.5 mol.L<sup>-1</sup> to remove  
179 excess of AO II. In order to release the adsorbed AO II, they were immersed in 10 mL of ultrapure  
180 water at pH 12 (adjusted with 0.5 mol.L<sup>-1</sup> NaOH) for at least 12 h at room temperature and under  
181 orbital agitation of 70 rpm and away from light. Then, the AO II concentration of solutions was  
182 determined by spectrophotometric titration with an UV-visible spectrometer at 485 nm after adjusting  
183 the pH to 3 by adding 1 mL of 0.1 mol.L<sup>-1</sup> HCl solution in each sample. The amount of amino groups  
184 grafted on the surface was calculated from a calibration curve generated with AO II solutions of  
185 known concentrations according to the following formula:

$$186 \quad -NH_2 (\mu mol. cm^{-2}) = \frac{Absorbance . Volume (mL)}{Slope (mL. \mu mol^{-1}) . Surface (cm^2)}$$

187

#### 188 **2.4.5. Colorimetric quantification of catecholamine groups**

189 Evidence of a pDA coating on raw scaffolds was reliably achieved using a simple and reliable method  
190 that is micro-bicinchoninic acid (micro-BCA assay). Investigations evidenced the success of detecting  
191 thin layers of pDA on different surfaces using this simple colorimetric test (Cho et al., 2014; Lih,  
192 Choi, Ahn, Joung & Han, 2016). Indeed, it is expected that amino groups of pDA can readily react  
193 with a bicinchoninic acid (BCA) based protein assay reagent, as when pDA-coated materials are  
194 exposed to test reagent, an attractive violet colour, due to the reduction reaction of Cu<sup>2+</sup> ions to Cu<sup>+</sup>, is  
195 generated. Control (unmodified) and functionalized nanofibers of 6 mm diameter were placed into a  
196 microplate well (96 wells microplate), treated with 150 μL of the freshly prepared microBCA working  
197 reagent (as instructed by the manufacturer) (Thermofisher Scientific, France) and incubated for 2 h  
198 at 37°C. Absorbance was measured at 562 nm using a multiwall plate reader (microplate fluorometer  
199 (TwinkleTMLB 970; Berthold Technologies GmbH & Co, Germany).

#### 200 **2.4.6. Vapour sorption isotherms**

201 The water sorption-desorption isotherms of samples were measured with a thermogravimetric analyser  
202 (Q5000 SA, TA Instruments, Guyancourt, France), consisting of a microbalance in which the sample  
203 and reference pans were enclosed in a humidity and temperature-controlled chamber. The relative  
204 humidity (RH) was controlled by mixing appropriate proportions (regulated by mass-flow controllers)  
205 of dry (RH=0%) and water saturated (RH=100%) N<sub>2</sub> gas flows (global flow set to 200 mL.min<sup>-1</sup>) in  
206 the chamber. The temperature was controlled by Peltier elements.

207 Basically, the sample was first placed into the chamber and dried to 0% RH and 60°C until its weight  
208 was stabilized to 0.01% for 180 min. The chamber temperature was then decreased to 37°C and the  
209 humidity was increased stepwise with RH plateaus of 5% until RH value reached 95%. For each RH

210 plateau, the sample's weight was stabilized to 0.01% for a time period of 180 min. the water  
211 desorption isotherm was then registered by decreasing RH down to 0% with 5% RH increments.

## 212 **2.5. *In vitro* biomineralization of scaffolds**

213 1.5 x concentrated Simulated Body Fluid (1.5xSBF) solution was prepared according to Kokubo et al.  
214 (Kokubo & Takadama, 2006). Briefly, NaCl (213 mM), NaHCO<sub>3</sub> (6.3 mM), KCl (7.5 mM),  
215 K<sub>2</sub>HPO<sub>4</sub>·3H<sub>2</sub>O (1.5 mM), MgCl<sub>2</sub>·6H<sub>2</sub>O (2.3 mM), CaCl<sub>2</sub> (3.8 mM), Na<sub>2</sub>SO<sub>4</sub> (0.8 mM) and tris buffer  
216 (40 mM) were dissolved and stirred in ultrapure water. HCl (1 M) was added to the solution until  
217 reaching a pH of 7.4. Untreated and polydopamine treated nanofibers were immersed in 50 mL  
218 1.5xSBF in a flat flask at 37°C. The 1.5xSBF was refreshed every two days. After incubation for 7  
219 days, the scaffolds were taken out and gently washed with ultrapure water and air dried. The formation  
220 of apatite coating on the surface of polydopamine functionalized disks was observed using SEM  
221 (Hitachi S-4700 SEM field emission GU) at 5kV. Thermogravimetric analysis (TGA) was performed  
222 to highlight the presence of mineral phase within biomineralized scaffolds. Specifically, samples were  
223 placed into platinum pans and put into a TGA Q50 (TA Instruments), then heated from 30°C up to  
224 700°C at a heating rate of 10 °C per minute under nitrogen protection (90 mL.min<sup>-1</sup>). The crystalline  
225 phase of calcium phosphate precipitates was investigated by X-ray diffraction (XRD). XRD was  
226 performed using a X'Pert Pro MRD<sup>®</sup>, PANalytical. The diffractograms were obtained in the range of 5  
227 to 70° (steps of 0.02°, counting time 120 s), with a detector (X'Celegator<sup>®</sup>, PNAalytical) provided  
228 with an anti-divergence slot 0, 5° and 1° and a mask of 10 mm.

## 229 **2.6. *Cells proliferation test***

230 The proliferation of pre-osteoblast cell (MC3T3-E1, ATCC<sup>®</sup> CRL-2594TM, USA) on the surface of  
231 CHT nanofiber membranes was assessed by direct-contact experimental set-up. The CHT membrane  
232 disks (diameter 11 mm) were placed at the well bottom of 48 well cell culture multiwall plate and  
233 stabilized by rubber ring (Viton<sup>®</sup> O-rings, diameter 11 mm), and the well without membrane disk as  
234 control. 450 µL complete cell culture medium (CCM), which containing α-MEM (Gibco, France) with  
235 10% fetal bovine serum (Gibco, France) and 40 µg/mL gentamicin (Panpharma, France), was added to  
236 each well. Then a 50 µL drop cell suspension (at 1.6×10<sup>5</sup> cells/mL) of MC3T3-E1 cells were seeded in  
237 each well. The culture plate was incubated at 37°C, 5% CO<sub>2</sub> and 100% humidity for 3 days. The  
238 cellular viability was measured by the AlamarBlue<sup>®</sup> assay (ThermoFisher Scientific, France). Briefly,  
239 the CCM was removed from each well, and 500 µL of 10% AlamarBlue<sup>®</sup> in CCM was added, and  
240 incubated for 2 h avoiding the light. From each well, 150 µL AlamarBlue<sup>®</sup> solution was transferred  
241 into a 96-well plate (Fluoro-LumiNunc<sup>™</sup>, ThermoScientific, Illkirch-Graffenstaden, France). The  
242 intensity of fluorescence was determined using a Twinkle LB 970 Microplate Fluorometer (Berthold,  
243 Bad Wildbad, Germany) with an excitation wavelength of 530 nm and an emission wavelength of 590

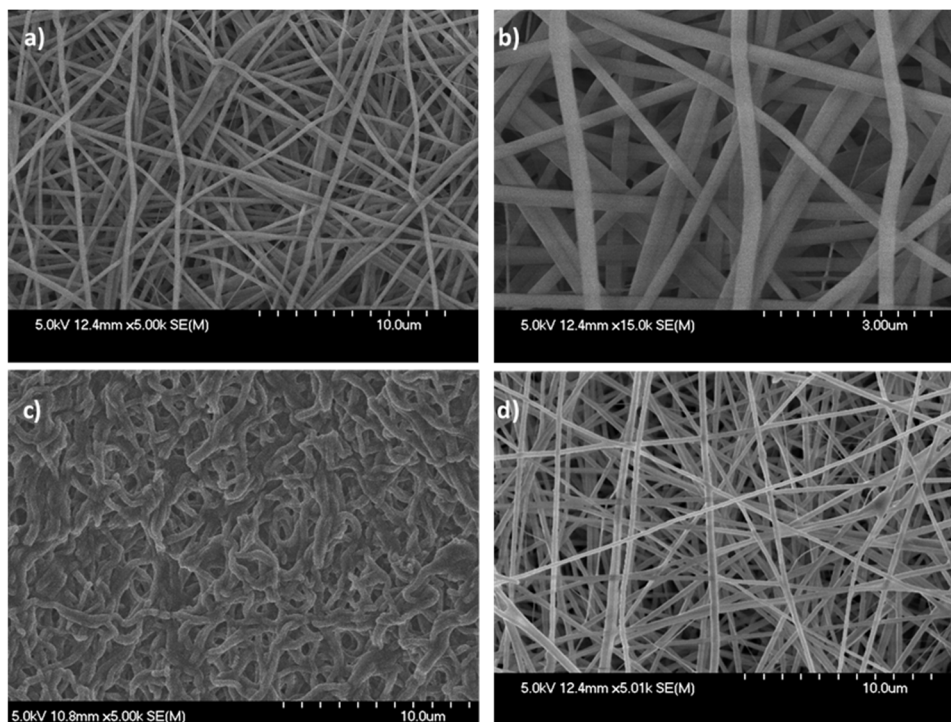


244 nm. The cell survival rate was expressed by the percentage of cell viability with respect to the value of  
245 the control.

### 246 3. Results and discussion

#### 247 3.1. Characterization of raw CHT nanofiber membranes

248 Electrospun CHT/ PEO nanofibrous scaffolds before and after crosslinking step by thermal treatment  
249 (140°C, 4h) are shown in Fig. 1.a. Bead-free nanofibers with average diameter of CHT/ PEO  
250 nanofibers present low polydispersity ( $247 \pm 36$  nm). However, as spun NFs in PBS solution (pH 7.4)  
251 swelled, merged and shrunk upon drying, leading to the decrease of the nanofibrous mats porosity  
252 (Fig. 1.a.c). On contrary, as displayed in Fig. 1.a.d, the nanofibrous structure of samples post-treated at  
253 140 °C for 4 hours was not affected. In the present case, the enhanced stability of the NFs in water  
254 after thermal treatment suggests the physical self-crosslinking of CHT. It is supposed that thermal  
255 treatment induced the dehydration of CHT within the NFs, promoting interchain hydrogen bondings,  
256 enhancing thereby NFs stability in PBS medium.



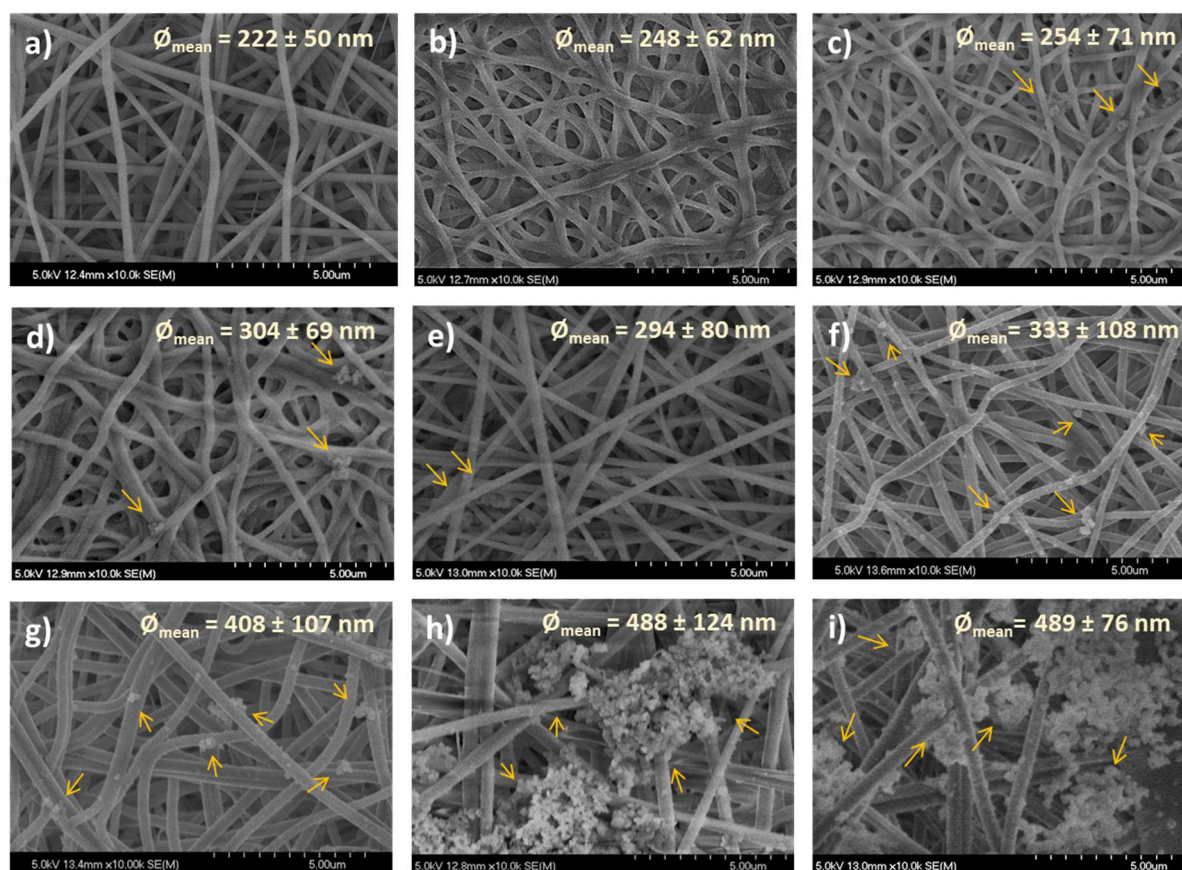
257  
258 **Figure 1** SEM images of CHT/PEO based nanofibers with a mass ratio of 90/10, a) before  $\times 5k$ ; b)  $\times$   
259 15k; c) after immersion in PBS solution at pH 7.4 for 24h ( $\times 5k$ ) before (c) and after (d) thermal  
260 treatment (TT) at 140° C for 4h after immersion in PBS ( $\times 5k$ ).

#### 261 3.2. Modification of CHT nanofibers with polydopamine

262 The polydopamine (pDA) deposit was first highlighted by the colour change of membranes, as the  
263 non-functionalized membrane darkened with increase of the immersion time in dopamine solution (see  
264 supplementary data, Fig. S1).

### 265 3.2.1. SEM analysis

266 SEM images shown in Fig. 2 displayed the preservation of nanofibers morphology and the porosity of  
267 the nanofibrous membrane even after immersion in dopamine solution and the increase of fibres mean  
268 diameter with time of functionalization, from  $222 \pm 50$  nm for raw NFs, up to  $489 \pm 76$  nm after 120  
269 hours of treatment. In addition, Fig. 2 also displays pDA particles appearing on samples treated with  
270 dopamine from reaction times superior to 48 hours (Fig. 2.f, g and h), forming well visible aggregates  
271 after 96 and 120 hours of functionalization (Fig. 2.h and i). These results are in agreement with those  
272 obtained by Shin *et al.* who studied the chemical modification of PCL nanofibers by PDA and  
273 evidenced that the surface morphology was dependent on the concentration of dopamine solution  
274 (Shin, Jun, Lim, Rhim & Shin, 2013). Indeed, these authors reported that scaffolds that have been  
275 immersed in a  $2 \text{ mg. mL}^{-1}$  dopamine solution contained very few pDA particles while a concentration  
276 of  $20 \text{ mg. mL}^{-1}$  provided nanofibers with higher quantity of pDA particles aggregates. We observed  
277 the same phenomenon in our case, as the SEM images in Fig. 2 display the appearance of pDA  
278 nanoparticles in the range of 100 nm from 2 hours of treatment (indicated by the arrows on the  
279 micrographs), and these nanoparticles formed aggregates well visible on samples treated during 96 and  
280 120 hours. This behaviour could be explained by the fact that dopamine spontaneously polymerizes  
281 on the nanofibers' surface by forming a thin layer of pDA, and that extending the treatment time led  
282 to homopolymerization of dopamine and precipitation of the insoluble pDA nanoparticles, firstly  
283 isolated on the scaffolds for treatment time up to 72 hours, and then forming aggregates. As a result, in  
284 order to limit the pores clogging of the scaffolds by pDA aggregates, an immersion time inferior or  
285 equal to 72 hours has been applied at this stage of the study.



286

287 **Figure 2** SEM images (x10k) of CHT-based nanofibers a) non-functionalized and functionalized with  
 288 polydopamine during b) 2h, c) 4h, d) 6h, e) 24h, f) 48h, g) 72h, h) 96h and i) 120h. The average  
 289 diameters of NFs are indicated in the respective figures. Arrows indicate polydopamine particles on  
 290 the surface of NFs

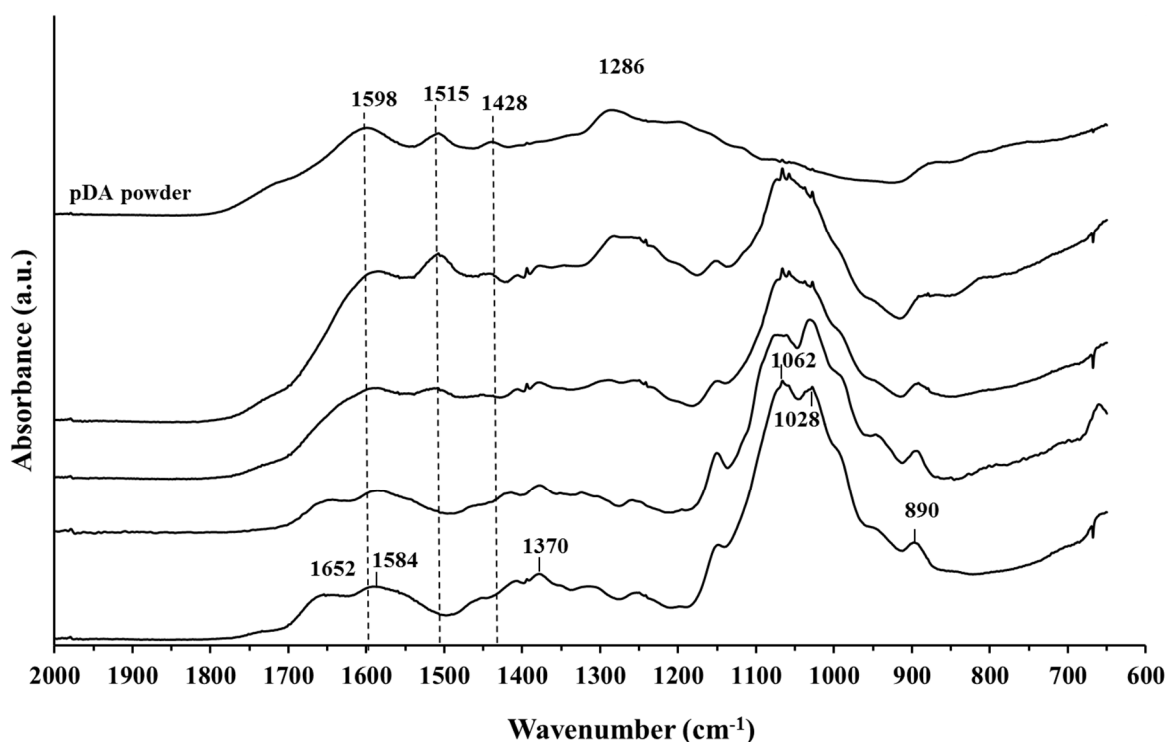
### 291 3.2.2. Characterization by FTIR

292 CHT-PEO (NFs CHT) and functionalized with pDA (NFs pDA) were characterized by attenuated total  
 293 reflection mode (ATR) FTIR and spectra were compared with that of pDA powder synthesized in  
 294 absence of NFs by self-polymerization of dopamine hydrochloride in pH 8.7 Tris buffer during 7  
 295 days. The black coloured precipitate in suspension was collected by filtration on 0.45 μm membrane  
 296 and analysed (Fig. 3). FTIR spectrum of CHT-based nanofibers displayed characteristic bands at 1653  
 297  $\text{cm}^{-1}$  and 1584  $\text{cm}^{-1}$  related to C=O elongation of amide groups (amide I band) and to N-H bending  
 298 vibration of primary amines in the glucosamine repeat units of CHT, respectively. The N-H bending of  
 299 amide groups (amide II band) appears at 1550  $\text{cm}^{-1}$ , shouldering the band aforementioned. The band  
 300 observed at 1370  $\text{cm}^{-1}$  corresponds to C-H symmetrical deformation of acetamide group, bands at  
 301 1062 and 1028  $\text{cm}^{-1}$  are related to the stretching of C-O and at 890  $\text{cm}^{-1}$  is related to the C-H bending  
 302 out of the plane of the ring of monosaccharides (Dimzon & Knepper, 2015).

303 Compared to raw CHT nanofibers, pDA-functionalized scaffolds during 48 and 96 hours displayed  
 304 increasing bands at 1598, 1428 and 1290  $\text{cm}^{-1}$  assigned to the overlap of C = C resonance vibrations

305 of aromatic cycles, and a peak at  $1515\text{ cm}^{-1}$  related to C - N vibrations confirming the presence of  
306 indole groups that are observed in the pDA nanoparticles' spectrum (Jiang, Zhu, Li, Xu & Zhu, 2010;  
307 Zangmeister, Morris & Tarlov, 2013). In addition, a decrease of the intensity of characteristic bands of  
308 CHT, in particular those at  $1652\text{ cm}^{-1}$  and at  $1062\text{ cm}^{-1}$ , is observed. FTIR could not evidence the  
309 immobilization of pDA after 2 hours of treatment as spectra of raw and treated NFs were similar,  
310 however it confirmed the presence of pDA on the scaffolds at 48 hours.

311



312

313 **Figure 3** IRTF-ATR spectra of raw chitosan-based nanofibers (NFs CHT), after functionalization with  
314 polydopamine (NFs pDA) during 2h, 48h and 96h and of polydopamine nanoparticles synthesized  
315 separately from NFs

### 316 3.2.3. Thermogravimetric analysis

317 Raw and functionalized membranes, as well as pDA powder were analysed by TGA (see  
318 **supplementary data, Fig. S2**). The thermogram of raw nanofibers showed a first mass loss between  
319  $25^{\circ}\text{C}$  and  $90^{\circ}\text{C}$  related to the loss of water that has been absorbed by the scaffold. A second mass loss  
320 at  $200^{\circ}\text{C}$  corresponding to the degradation of both CHT and PEO can be observed, as well as a third  
321 mass loss at  $320^{\circ}\text{C}$  attributed to a coal residue degradation. The pDA powder exhibited a mass loss  
322 between  $25^{\circ}\text{C}$  and  $80^{\circ}\text{C}$ , due to dehydration, and a complete degradation in a single step ranging from  
323  $200^{\circ}\text{C}$  up to  $600^{\circ}\text{C}$ . As a result, functionalized scaffolds displayed a first weight loss between 25 and  
324  $50^{\circ}\text{C}$  attributed to water loss and a second one between  $200^{\circ}\text{C}$  and  $500^{\circ}\text{C}$  related to the degradation of

325 PEO, CHT and pDA. Compared to raw membranes, the functionalized ones showed a shift due to the  
326 decomposition of pDA that occurs at a higher temperature than that of CHT. It is worth to notice that  
327 the degradation of both samples was complete (no residue).

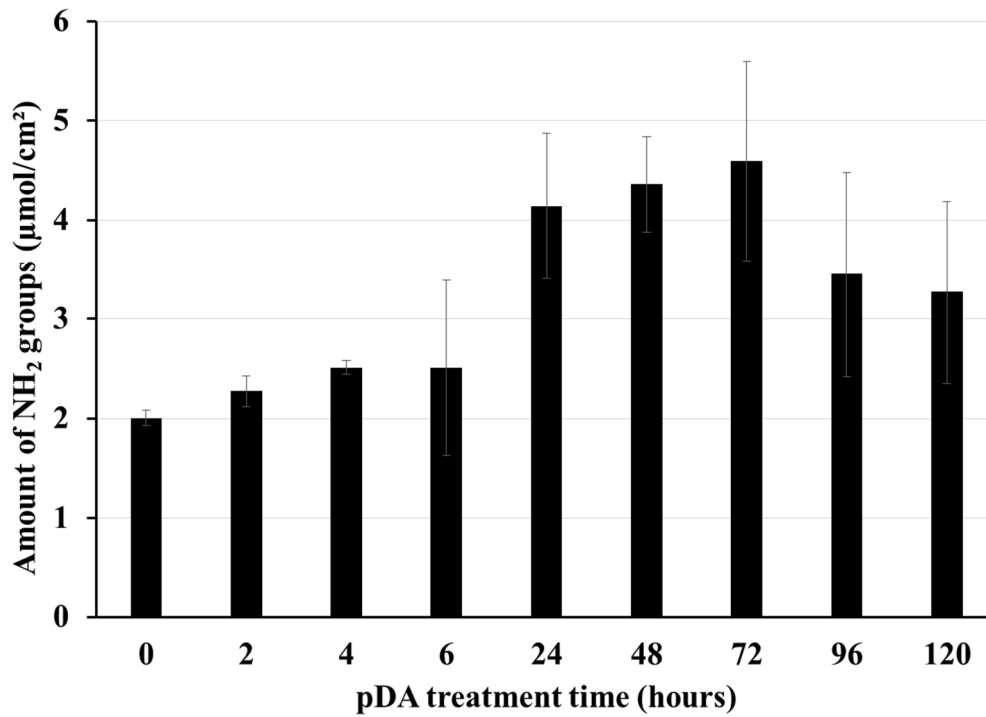
#### 328 **3.2.4. Titration of amino and catechol groups**

329 As observed in Figs. 4.a and 4.b, a parallel evolution of amino groups and catechol groups occurred  
330 with reaction time. The amount of amino groups available on the surface of scaffolds was measured  
331 using the Orange II assay (Fig. 4.a). Unmodified nanofibers showed an amount of  $2.0 \mu\text{mol.cm}^{-2}$  of  
332 amino groups and this value increased up to  $2.5 \mu\text{mol.cm}^{-2}$  after 6h,  $4.1 \mu\text{mol.cm}^{-2}$  after 24h until  
333 reaching a maximum  $4.6 \mu\text{mol.cm}^{-2}$  at 72 h of scaffolds immersion in the dopamine solution.  
334 However, a surface modification higher than three days caused an insignificant decrease of the amount  
335 of free amino groups down to  $4.2 \mu\text{mol.cm}^{-2}$  after 120h. It is supposed that this phenomenon was due  
336 to the presence of polydopamine nanoparticles aggregates observed on SEM images in Fig. 2 that  
337 could reduce the availability toward Orange II of free amines present inside those aggregates.

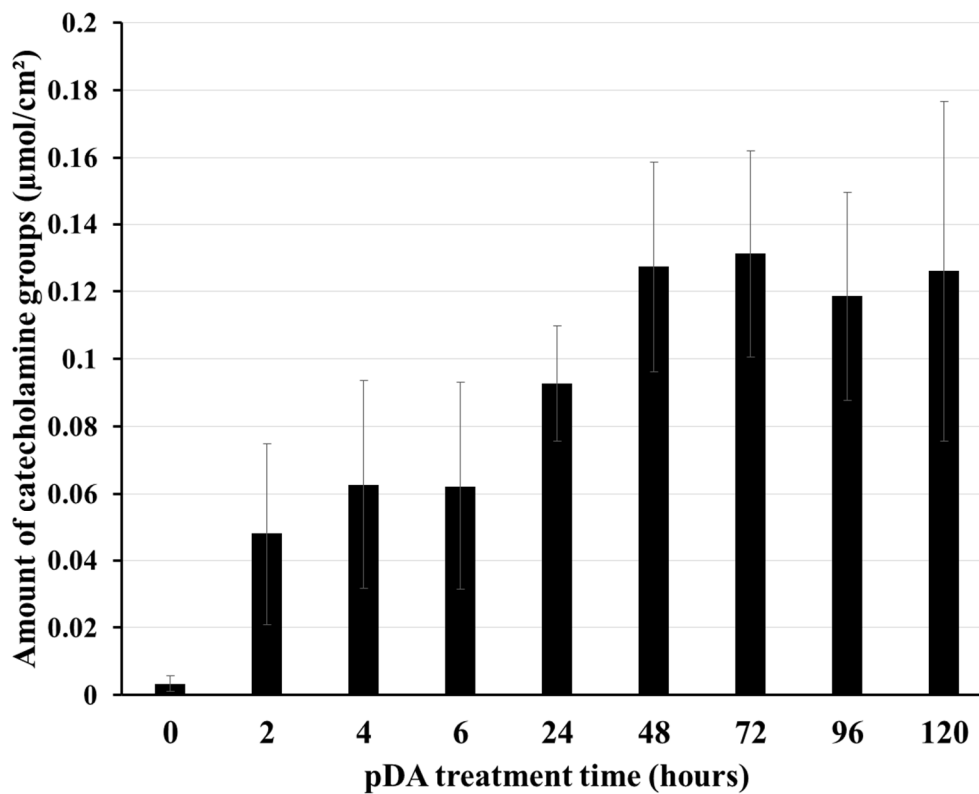
338 Elsewhere, lower range of values of amino groups were measured by Kang *et al.* on bulk metal  
339 supports made of titanium and stainless steel (Kang et al., 2012). These authors reported presence of  
340 only  $1.875$  and  $3.125 \text{ nmol.cm}^{-2}$  of amino groups respectively on smooth surfaces of titanium and  
341 stainless-steel treated by dopamine during 24h. Our group also reported similar results with the  
342 presence of  $6.0 \text{ nmol.cm}^{-2}$  on vascular stents modified with pDA (Sobocinski et al., 2014). Such  
343 differences can be explained by the very higher specific surface of nanofibrous mats compared to that  
344 of smooth surfaces of bulk materials on the one hand, and also to the different surface reactivity of  
345 CHT toward dopamine, compared to metals.

346 The titration of catechol groups by the micro-BCA colorimetric test (Fig. 4.b) displays an increase  
347 from  $0.048$  to  $0.131 \mu\text{mol.cm}^{-2}$  for samples treated by dopamine during 2h and 72h respectively. Then,  
348 a slight decrease of catechol groups density for immersion times higher than 72h can be noticed,  
349 probably due to the presence of polydopamine aggregates formed in the nanofibrous network, as  
350 suggested above.

a



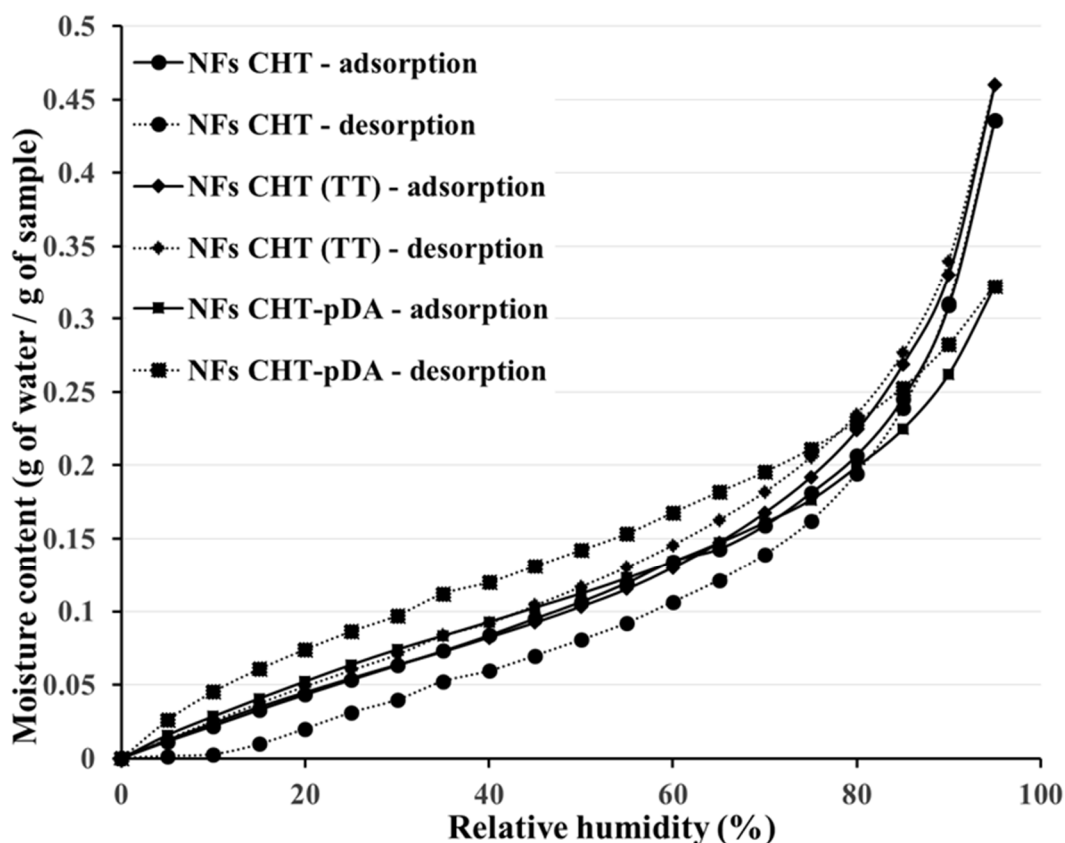
b



351  
352 **Figure 4** Quantification expressed in  $\mu\text{mol}/\text{cm}^2$  of amine groups (4.a) and catecholamine groups (4.b)  
353 on CHT NFs treated with different immersion times in polydopamine solutions ranging from 0h  
354 (control samples) up to 120h (n = 3).

355 **3.2.5. Vapour sorption measurements**

356 A water vapour sorption study was achieved on CHT/ PEO nanofibrous scaffolds before and after  
 357 thermal post-treatment of NFs and after treatment with pDA (Fig. 5). Sorption and desorption curves  
 358 displayed a similar behaviour with linear responses between 0% and 75% of relative humidity (RH),  
 359 and exponential variation between 75% and 95% of humidity. A maximum of 435.6 mg and 459.8 mg  
 360 of water uptake per gram of sample before and after thermal treatment, was respectively observed.  
 361 Interestingly, water desorption cycle trace on untreated NFs was below that of adsorption while the  
 362 opposite was observed on thermally treated NFs. This confirms that thermal treatment of NFs at 160°C  
 363 induced a change of the physicochemical properties of NFs. Besides, the effect of polydopamine  
 364 treatment on water vapour sorption of nanofibers was evidenced as observed in Fig. 1B. As a matter  
 365 of fact, the water absorption and desorption measurements of unmodified and functionalized scaffolds  
 366 by pDA are presented in Fig. 5. Water vapour uptake by membranes before and after pDA treatment  
 367 decreased from 459.8 down to 322.3 mg of water / g of sample when HR was about 95%. For RHs  
 368 between 0 and 80%, the two samples have similar water adsorption profiles, and above 80%, the  
 369 moisture content of the CHT nanofibers has become greater than that of modified nanofibers.  
 370 Consequently, this result shows that the functionalization step of CHT NFs by pDA has caused a  
 371 decrease in NFs' swellability in water

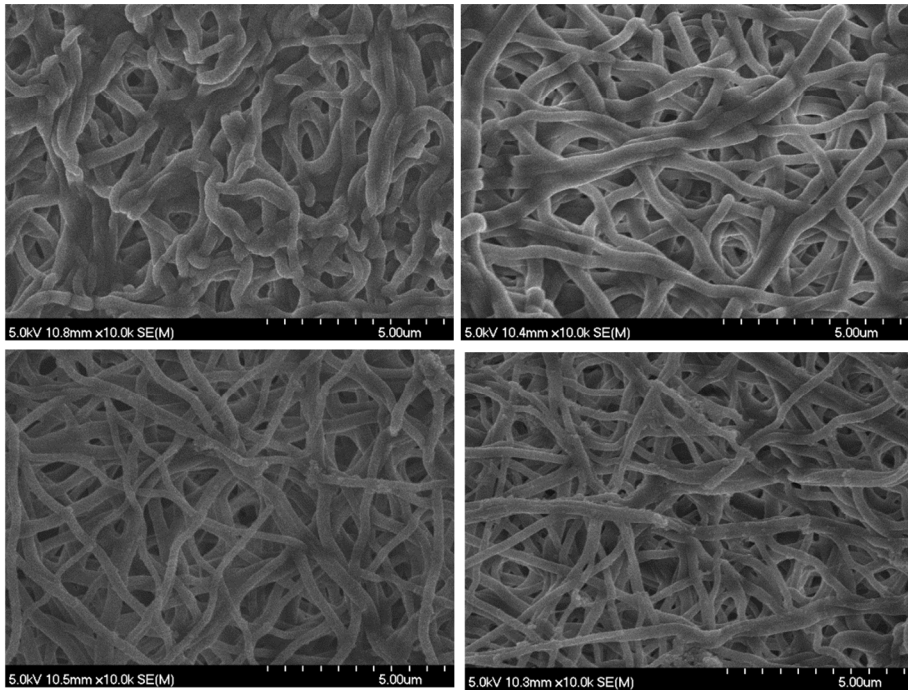
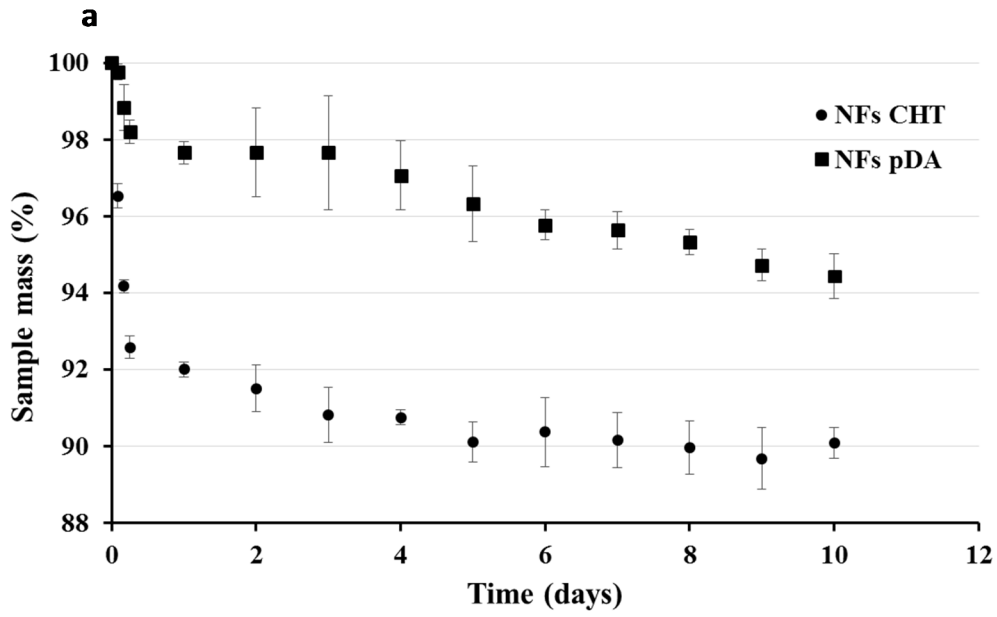


372  
 373 **Figure 5** Water vapor absorption isotherms of as spun CHT nanofibers before and after thermal  
 374 treatment (TT) and after treatment with pDA

375 **3.2.6. Degradation in PBS batch**

376 Fig. 6.a shows the degradation profiles of the samples in PBS batch at 37°C. A first fast degradation  
377 phase, up to one day, and a second slower second phase can be observed of both profiles. In the first  
378 phase, a significant loss of mass of 8% and 2% for CHT NFs and CHT/ pDA NFs, respectively, was  
379 noticed. We previously reported that this weight loss could be assigned to the PEO dissolution in the  
380 PBS batch as CHT nanofibers were initially prepared from the electrospun solution containing 9:1  
381 CHT-PEO weight ratio. This was evidenced by a proton NMR analysis of the freeze-dried residue of  
382 the PBS degradation medium which displayed the NMR signal of PEO released from the CHT-PEO  
383 NFs (Ouerghemmi et al., 2016). Further, the kinetics of degradation process was slowed down after 10  
384 days until reaching 10% and 6% of mass loss, respectively. Therefore, the polydopamine coating  
385 allowed to stabilize and delay degradation of nanofiber membranes. These results are confirmed by a  
386 SEM observation since swelling of CHT nanofibers could be observed at the beginning of the  
387 degradation (2 hours) (Fig. 6.b). While fibrous and porous morphology is retained for modified  
388 nanofibers that have lost their straightness.



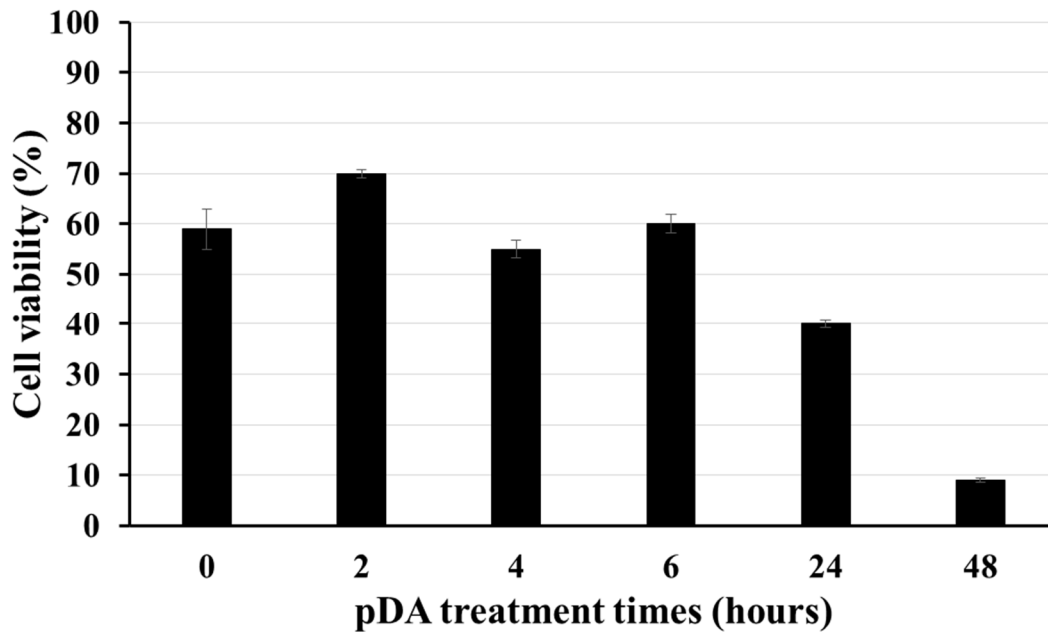


389

390 **Figure 6** Degradation of as spun and pDA functionalized nanofibers (n = 3) expressed by their weight  
 391 percentage in function of time in PBS batch at 37°C (6.a), SEM images of samples after 2h and 5 days  
 392 in PBS batch (x10k) (6.b).

393 **3.2.7 Cytocompatibility study**

394



395  
 396 Figure 7 Viability of cells MC3T3-E1 in contact with NFs before (0h) and after pDA treatment  
 397 during 2 to 48 hours by direct contact method (n=3) after 3 days of incubation. TCPS was used as  
 398 control corresponding to a viability of 100%.

399 The cytocompatibility of samples treated with dopamine during times varying from 2 hours up to 48  
 400 hours was assessed in presence of MC3T3-E1 cells by the direct contact method. Figure 7 displays a  
 401 cells viability of 70% for a treatment time of 2 hours, then viability decreased down to 60% after 6  
 402 hours, 40% after one day and levelled off at 8% after 2 days. It is known from literature that pDA  
 403 especially in the shape of nanoparticles may provoke a cytotoxic effect. For example Nieto *et al.*  
 404 studied in depth this phenomenon with tumor cells cultures (Nieto, Vega, Enrique, Marcelo & Martín  
 405 Del Valle, 2019). As a matter of fact, the SEM study reported in an above section (Fig. 2) displayed  
 406 the formation of pDA nanoparticles on NFs samples from reaction time of 4 hours in the dopamine  
 407 batch. So this confirms that the decrease of the viability above 2 hours of treatment can be correlated  
 408 with the formation of pDA nanoparticles. Finally, this experiment allowed us to fix the pDA treatment  
 409 time to 2 hours for the preparation of scaffolds for their *in vitro* biomineralization described in the next  
 410 section.

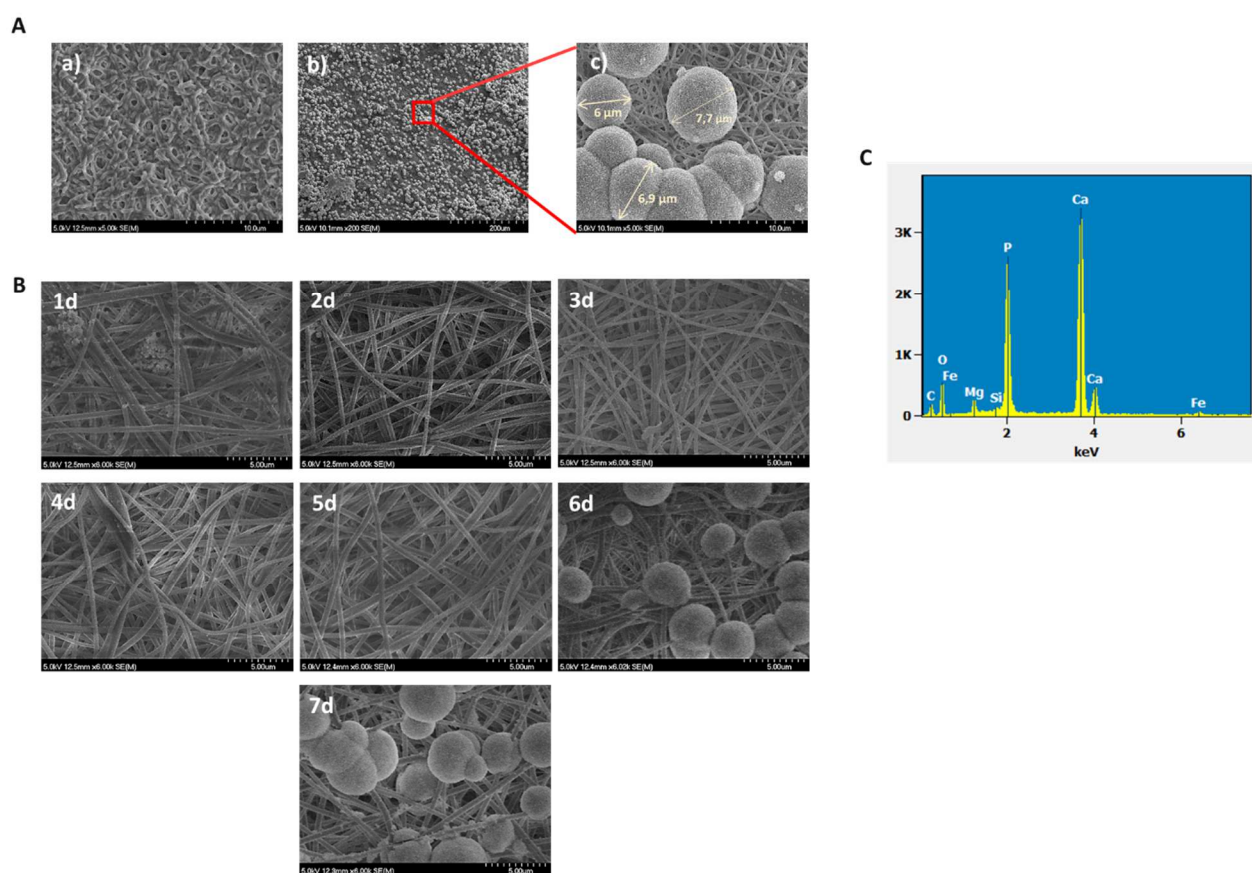
411  
 412 **3.3. *In vitro* biomineralization of CHT-pDA scaffolds**

413 The ability of the NFs to induce the formation of calcium phosphate (CaP) was evaluated *in vitro* by  
 414 immersing the samples in a solution of 1.5×SBF for up to 7 days with renewing the solution every 48  
 415 h. Fig. 8.A displays that the surface of the nanofibrous scaffold previously functionalized with pDA  
 416 for 2 h, is fully covered with spherical shaped CaP particles in contrast with the as spun CHT which  
 417 does not display any particles formation (Fig. 8.A.a). As observed in Fig. 8.A.c), the spherical  
 418 particles present a diameter in the range of 7  $\mu\text{m}$ . Fig. 8B displays the evolution of NFs-pDA

419 scaffolds from the first to the seventh day in contact with SBF and evidences that biomineralization  
420 occurred from the 6<sup>th</sup> day.

421 After the complete pyrolysis of the organic part (CHT and pDA) observable up to 600°C, the TGA  
422 analysis of the biomineralized scaffolds displayed the presence of a mineral residue corresponding to  
423 17% of the initial weight (See Fig. S3 in supplementary data).

424 Energy dispersive spectroscopy (EDS) microanalysis (Fig.8.C) displayed the presence of Ca and P  
425 elements on the biomineralized scaffolds. Calculated from their respective relative abundances the  
426 Ca/P ratio is 1.76. This value is close to that of hydroxyapatite whose Ca / P ratio is 1.67.  
427 Nevertheless, this study is semi-quantitative and does not allow us to affirm the presence of  
428 hydroxyapatite in its pure state.



429  
430

431 **Figure 8** SEM images of CHT nanofibers obtained after 7 days in SBF NFs as spun (without pDA  
432 coating) (magnification x5k) (8.A.a), NFs functionalized with pDA for 2h (magnification x200)  
433 (8.A.b), and (magnification x5k) (8.A.c) ; SEM images of nanofibers functionalized with pDA and  
434 then biomineralized for 1 up to 7 days (magnification x6k) (8.B); EDS spectrum of membranes after  
435 immersion in 1.5×SBF solution (8.C)

436 The biom mineralized NFs surface was analysed by FTIR in total reflection mode (Fig. 9.a). The  
437 spectrum of HA powder is also displayed in order to highlight its characteristic peaks.

438

439 Spectrum of NFs-pDA supporting CaP crystals displays a strong double band in the region 2920 -  
440 2880  $\text{cm}^{-1}$  which can be attributed to  $\text{CH}_2$  asymmetric and symmetric stretching, typical of  
441 polysaccharides. However, in the lower region of the spectrum, the signal of the calcium phosphate  
442 covering the scaffold overlaps the vibration bands relative to non-biom mineralized NFs-pDA sample  
443 (detailed in section 3.2.2 and Fig. 3). The vibrations bands of  $\nu_3 \text{PO}_4^{3-}$  group (asymmetric elongation  
444 of P-O) appears clearly at 1000-1100  $\text{cm}^{-1}$  (large band) and shouldering symmetric  $\nu_1 \text{PO}_4^{3-}$  at 960  $\text{cm}^{-1}$ .  
445 The peak observed at 880  $\text{cm}^{-1}$  and the wide band at 1420-1470  $\text{cm}^{-1}$  reflect the presence of traces of  
446 carbonate ions. The weak band at 1630  $\text{cm}^{-1}$  corresponds to free water (Kokubo & Takadama, 2006).

447 These results have been supplemented with a X-ray diffractometry (XRD) analysis in order to define  
448 more finely the nature of the calcium phosphate nodules formed upon the biom mineralization step. Fig.  
449 9.b shows the different diffractograms of NFs after both pDA and biom mineralization steps of the  
450 process (green and blue plots respectively). A peak at  $2\theta = 20^\circ$  corresponding to CHT (020 diffraction  
451 plane), the main constituent of nanofiber scaffolds, was noticed and the shoulder observed at  $2\theta = 28^\circ$   
452 was attributed to PEO present in the precursor electrospun CHT solution (Ouerghemmi et al., 2016)

453

454 In addition, the spectrum of the mineral residue of biom mineralized sample during 7days before (blue  
455 plot) and after calcination (red plot) is displayed.

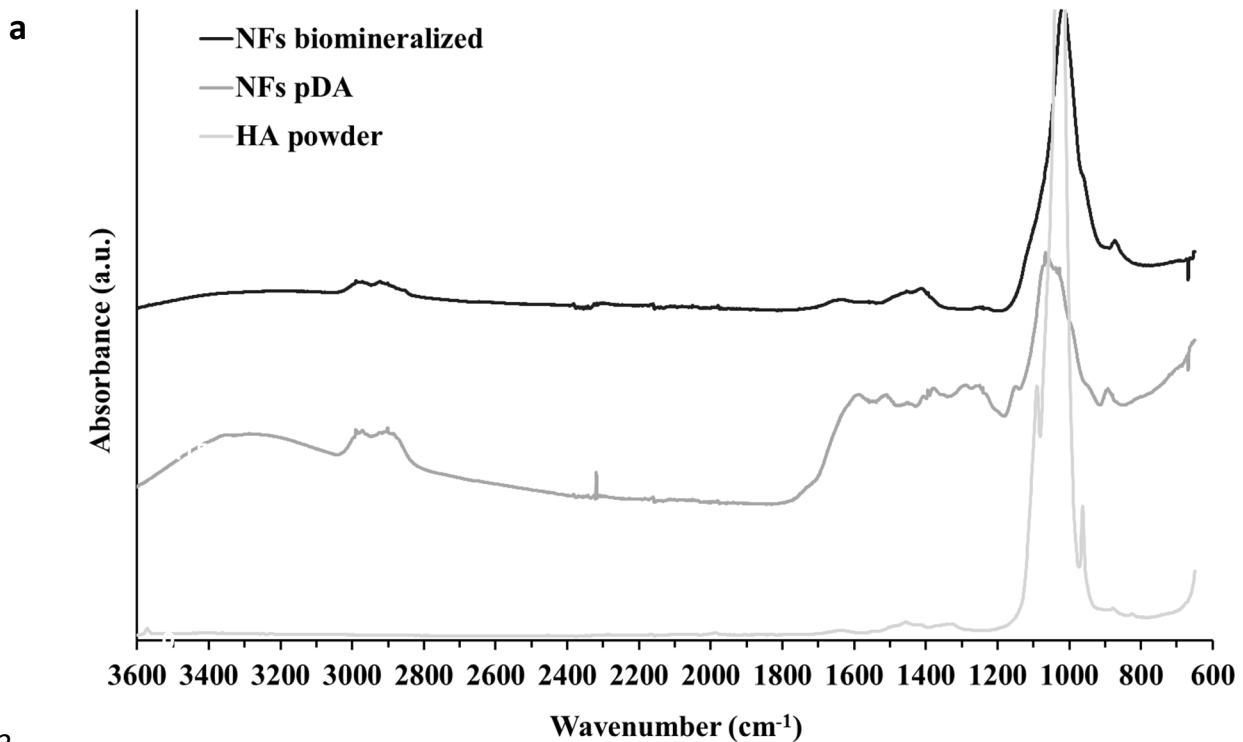
456 In addition, the diffractograms of biom mineralized nanofibers before calcination (curve in blue) showed  
457 a slight shoulder at  $2\theta=32^\circ$  revealing the presence of an apatitic phase. The XRD spectrum of the  
458 solid residue resulting from calcination of a biom mineralized membrane (during 7d in 1.5xSBF) days  
459 displayed well defined narrow peaks revealing the presence of a crystalline phase. As a matter of fact,  
460 the spectrum of the calcined residue corresponds to a superposition of the spectrum of pure  
461 hydroxyapatite (majority) as well as spectra of other calcium phosphates such as whitlockite and  
462 magnesium and calcium phosphate (minor) (see supplementary data, Fig. S4 and Fig. S5). So, due to  
463 the low percentage of crystallinity of the bio-mineralized phase it is not possible to correctly determine  
464 the main angles and diffraction planes of this phase (blue plot), only the presence of chitosan seems  
465 visible by XRD. However, after calcination at 1000  $^\circ\text{C}$  of biom mineralized nanofibers (red plot) we  
466 clearly see the peaks of calcium phosphate with the peak 100% of hydroxyapatite (plane 211,  $2\theta =$   
467  $31.773^\circ$ ) and the peak 100% of whitlockite (plane 0210,  $2\theta = 31.026^\circ$ ).

468

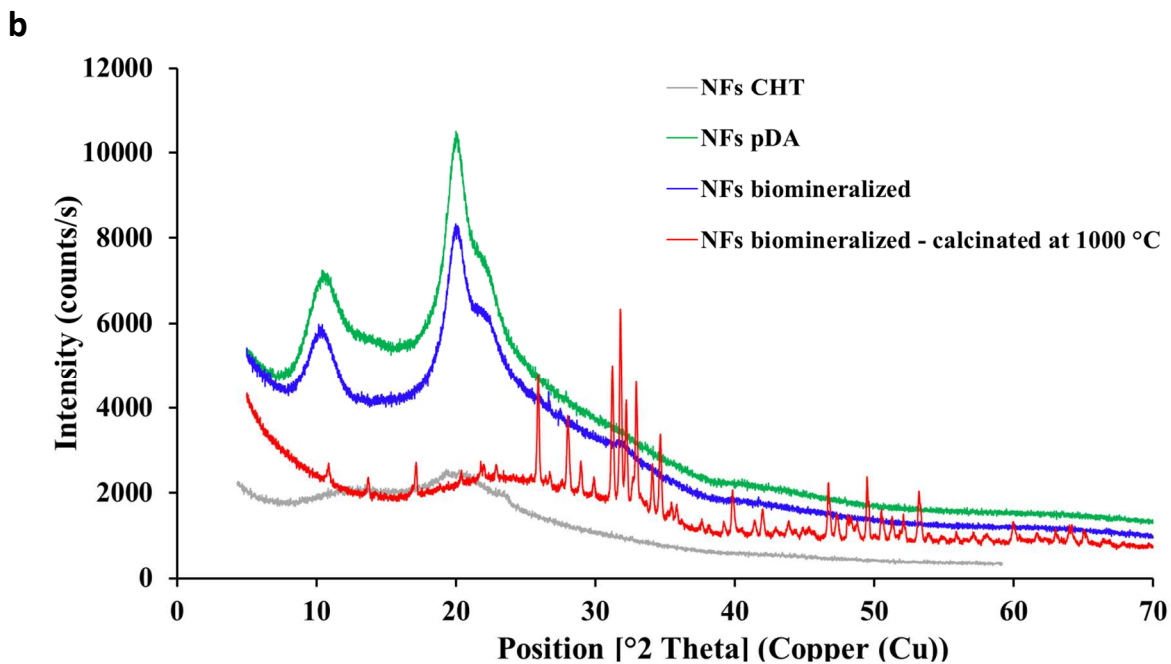
469

470

471



472



473

474 **Figure 9** IRTF-ATR spectra of pure powder of hydroxyapatite and nanofibers modified with pDA for  
475 2h and after biom mineralization during 7 days (9.a), Diffractograms of raw membranes (grey),  
476 functionalized nanofibers with pDA before (green) and after (blue) biom mineralization process for 7d,  
477 calcination residue of biom mineralized membrane after 7 d (red) (9.b).

478

#### 479 **4. Conclusion**

480 This work firstly described the treatment of chitosan nanofibrous scaffolds by polydopamine (NFs-  
481 pDA) by applying increasing reaction times. FTIR and titration analyses displayed the increase of  
482 pDA layer on the CHT NFs up to 48 h. The SEM study revealed the presence of large pDA  
483 nanoparticles aggregates for treatment times more than 72 h. We observed that pDA treatment time of  
484 2 h was the best compromise between i) the stabilization effect of NFs in PBS pH 7.4 medium, ii) the  
485 cytocompatibility in presence of MC3T3-E1 pre-osteoblast cells and iii) the ability of the scaffolds to  
486 biomineralize in 1.5xSBF medium.

487

488 As a matter of fact, after 6-day immersion in the 1.5xSBF solution, the formation of a mineralized  
489 layer composed of sphere-shaped nodules was observable by SEM. SEM-EDX and XPS analyses  
490 displayed this mineral phase was mainly composed of hydroxyapatite. The next steps of this study will  
491 be to study *in vitro* the proliferation, activity of alkaline phosphatase, osteogenesis-related proteins  
492 secretion of stem cells on the NFs-pDA scaffolds, and demonstrate thereby that this simple, bio-  
493 inspired surface modification of the NFs scaffold by pDA is a very encouraging tool for regulating cell  
494 behaviour, and may serve as an effective cell carrier for bone tissue engineering in the field of  
495 orthopaedic and dental applications. In particular, it will be interesting to investigate *in vivo* the  
496 process of bone reconstruction accomplished by the mineralisation process in concert with the  
497 biological action of bone-forming cells colonizing the scaffolds and the parallel progressive  
498 replacement of the bioresorbable NFs by new-formed bone.

499

#### 500 **Acknowledgments**

501 European Metropolis of Lille (MEL), Faculty of Sciences and Technologies of University of Lille,  
502 Region Hauts-de-France and Chevreul Institute (FR 2638) are acknowledged for supporting and  
503 funding this work.

#### 504 **References**

- 505 Balagangadharan, K., Dhivya, S., & Selvamurugan, N. (2017). Chitosan based nanofibers in bone  
506 tissue engineering. *International Journal of Biological Macromolecules*, *104*, 1372-1382.
- 507 Bose, S., Robertson, S. F., & Bandyopadhyay, A. (2018). Surface modification of biomaterials and  
508 biomedical devices using additive manufacturing. *Acta Biomaterialia*, *66*, 6-22.
- 509 Chen, S., Li, R., Li, X., & Xie, J. (2018). Electrospinning: An enabling nanotechnology platform for drug  
510 delivery and regenerative medicine. *Advanced Drug Delivery Reviews*, *132*, 188-213.
- 511 Chen, X., Nouri, A., Li, Y., Lin, J., Hodgson, P. D., & Wen, C. e. (2008). Effect of surface roughness of Ti,  
512 Zr, and TiZr on apatite precipitation from simulated body fluid. *Biotechnology and  
513 Bioengineering*, *101*(2), 378-387.

514 Chen, Z., Song, Y., Zhang, J., Liu, W., Cui, J., Li, H., & Chen, F. (2017). Laminated electrospun nHA/PHB-  
515 composite scaffolds mimicking bone extracellular matrix for bone tissue engineering. *Materials*  
516 *Science and Engineering: C*, *72*, 341-351.

517 Cho, H.-j., Madhurakkat Perikamana, S. K., Lee, J.-h., Lee, J., Lee, K.-M., Shin, C. S., & Shin, H. (2014).  
518 Effective Immobilization of BMP-2 Mediated by Polydopamine Coating on Biodegradable  
519 Nanofibers for Enhanced in Vivo Bone Formation. *ACS Applied Materials & Interfaces*, *6*(14),  
520 11225-11235.

521 Chong, L. H., Zarith, N. Z., & Sultana, N. (2015). Poly(Caprolactone)/chitosan-based scaffold using  
522 freeze drying technique for bone tissue engineering application. *2015 10th Asian Control*  
523 *Conference (ASCC)* (pp. 1-4).

524 Ciapetti, G., Granchi, D., Devescovi, V., Baglio, S. R., Leonardi, E., Martini, D., Jurado, M. J., Olalde, B.,  
525 Armentano, I., Kenny, J. M., Walboomers, F. X., Alava, J. I., & Baldini, N. (2012). Enhancing  
526 Osteoconduction of PLLA-Based Nanocomposite Scaffolds for Bone Regeneration Using Different  
527 Biomimetic Signals to MSCs. *International Journal of Molecular Sciences*, *13*(2).

528 Dimzon, I. K. D., & Knepper, T. P. (2015). Degree of deacetylation of chitosan by infrared  
529 spectroscopy and partial least squares. *International Journal of Biological Macromolecules*, *72*,  
530 939-945.

531 Ehrbar, M., Lütolf, M. P., Rizzi, S. C., Hubbell, J. A., & Weber, F. E. (2008). Artificial extracellular  
532 matrices for bone tissue engineering. *Bone*, *42*, S72.

533 Flores, C., Degoutin, S., Chai, F., Raoul, G., Hornez, J.-C., Martel, B., Siepmann, J., Ferri, J., &  
534 Blanchemain, N. (2016). Gentamicin-loaded poly(lactic-co-glycolic acid) microparticles for the  
535 prevention of maxillofacial and orthopedic implant infections. *Materials Science and*  
536 *Engineering: C*, *64*, 108-116.

537 Frohbergh, M. E., Katsman, A., Botta, G. P., Lazarovici, P., Schauer, C. L., Wegst, U. G. K., & Lelkes, P. I.  
538 (2012). Electrospun hydroxyapatite-containing chitosan nanofibers crosslinked with genipin for  
539 bone tissue engineering. *Biomaterials*, *33*(36), 9167-9178.

540 Gupta, K. C., Haider, A., Choi, Y.-r., & Kang, I.-k. (2014). Nanofibrous scaffolds in biomedical  
541 applications. *Biomaterials Research*, *18*(1), 5.

542 Haider, A., Haider, S., & Kang, I.-K. (2018). A comprehensive review summarizing the effect of  
543 electrospinning parameters and potential applications of nanofibers in biomedical and  
544 biotechnology. *Arabian Journal of Chemistry*, *11*(8), 1165-1188.

545 Ho, C.-C., & Ding, S.-J. (2014). Structure, Properties and Applications of Mussel-Inspired  
546 Polydopamine. *Journal of Biomedical Nanotechnology*, *10*(10), 3063-3084.

547 Hu, C., Ashok, D., Nisbet, D. R., & Gautam, V. (2019). Bioinspired surface modification of orthopedic  
548 implants for bone tissue engineering. *Biomaterials*, *219*, 119366.

549 Jang, J.-H., Castano, O., & Kim, H.-W. (2009). Electrospun materials as potential platforms for bone  
550 tissue engineering. *Advanced Drug Delivery Reviews*, *61*(12), 1065-1083.

551 Jiang, J.-H., Zhu, L.-P., Li, X.-L., Xu, Y.-Y., & Zhu, B.-K. (2010). Surface modification of PE porous  
552 membranes based on the strong adhesion of polydopamine and covalent immobilization of  
553 heparin. *Journal of Membrane Science*, *364*(1), 194-202.

554 Jiang, T., Deng, M., James, R., Nair, L. S., & Laurencin, C. T. (2014). Micro- and nanofabrication of  
555 chitosan structures for regenerative engineering. *Acta Biomaterialia*, *10*(4), 1632-1645.

556 Jiao, Y.-P., & Cui, F.-Z. (2007). Surface modification of polyester biomaterials for tissue engineering.  
557 *Biomedical Materials*, *2*(4), R24-R37.

558 Kang, J., Sakuragi, M., Shibata, A., Abe, H., Kitajima, T., Tada, S., Mizutani, M., Ohmori, H., Ayame, H.,  
559 Son, T. I., Aigaki, T., & Ito, Y. (2012). Immobilization of epidermal growth factor on titanium and  
560 stainless steel surfaces via dopamine treatment. *Materials Science and Engineering: C*, *32*(8),  
561 2552-2561.

562 Khajavi, R., Abbasipour, M., & Bahador, A. (2016). Electrospun biodegradable nanofibers scaffolds for  
563 bone tissue engineering. *Journal of Applied Polymer Science*, *133*(3).

564 Ko, E., Yang, K., Shin, J., & Cho, S.-W. (2013). Polydopamine-Assisted Osteoinductive Peptide  
565 Immobilization of Polymer Scaffolds for Enhanced Bone Regeneration by Human Adipose-  
566 Derived Stem Cells. *Biomacromolecules*, *14*(9), 3202-3213.

567 Kokubo, T. (1991). Bioactive glass ceramics: properties and applications. *Biomaterials*, *12*(2), 155-163.

568 Kokubo, T., & Takadama, H. (2006). How useful is SBF in predicting in vivo bone bioactivity?  
569 *Biomaterials*, *27*(15), 2907-2915.

570 Kwak, S., Haider, A., Gupta, K. C., Kim, S., & Kang, I.-K. (2016). Micro/Nano Multilayered Scaffolds of  
571 PLGA and Collagen by Alternately Electrospinning for Bone Tissue Engineering. *Nanoscale*  
572 *Research Letters*, *11*(1), 323.

573 Kwon, G., Kim, H., Gupta, K. C., & Kang, I.-K. (2018). Enhanced Tissue Compatibility of  
574 Polyetheretherketone Disks by Dopamine-Mediated Protein Immobilization. *Macromolecular*  
575 *Research*, *26*(2), 128-138.

576 Lee, H., Dellatore, S. M., Miller, W. M., & Messersmith, P. B. (2007). Mussel-Inspired Surface  
577 Chemistry for Multifunctional Coatings. *Science (New York, N.Y.)*, *318*(5849), 426-430.

578 Lee, S. J., Lee, D., Yoon, T. R., Kim, H. K., Jo, H. H., Park, J. S., Lee, J. H., Kim, W. D., Kwon, I. K., & Park,  
579 S. A. (2016). Surface modification of 3D-printed porous scaffolds via mussel-inspired  
580 polydopamine and effective immobilization of rhBMP-2 to promote osteogenic differentiation  
581 for bone tissue engineering. *Acta Biomaterialia*, *40*, 182-191.

582 Levenson, S. K. L., & Zhang, M. (2014). Chitosan-based scaffolds for bone tissue engineering. *Journal*  
583 *of Materials Chemistry B*, *2*(21), 3161-3184.

584 Liao, S., Murugan, R., Chan, C. K., & Ramakrishna, S. (2008). Processing nanoengineered scaffolds  
585 through electrospinning and mineralization suitable for biomimetic bone tissue engineering.  
586 *Journal of the Mechanical Behavior of Biomedical Materials*, *1*(3), 252-260.

587 Lih, E., Choi, S. G., Ahn, D. J., Joung, Y. K., & Han, D. K. (2016). Optimal conjugation of catechol group  
588 onto hyaluronic acid in coronary stent substrate coating for the prevention of restenosis. *Journal*  
589 *of Tissue Engineering*, *7*, 2041731416683745.

590 Liu, H., Li, W., Wen, W., Luo, B., Liu, M., Ding, S., & Zhou, C. (2017). Mechanical properties and  
591 osteogenic activity of poly(L-lactide) fibrous membrane synergistically enhanced by chitosan  
592 nanofibers and polydopamine layer. *Mater Sci Eng C Mater Biol Appl*, *81*, 280-290.

593 Liu, Y., Cui, H., Zhuang, X., Wei, Y., & Chen, X. (2014). Electrospinning of aniline pentamer-graft-  
594 gelatin/PLLA nanofibers for bone tissue engineering. *Acta Biomaterialia*, *10*(12), 5074-5080.

595 LogithKumar, R., KeshavNarayan, A., Dhivya, S., Chawla, A., Saravanan, S., & Selvamurugan, N. (2016).  
596 A review of chitosan and its derivatives in bone tissue engineering. *Carbohydrate Polymers*, *151*,  
597 172-188.

598 Lyng, M. E., van der Westen, R., Postma, A., & Städler, B. (2011). Polydopamine—a nature-inspired  
599 polymer coating for biomedical science. *Nanoscale*, *3*(12), 4916-4928.

600 Ma, X., Wu, G., Dai, F., Li, D., Li, H., Zhang, L., & Deng, H. (2021). Chitosan/polydopamine layer by  
601 layer self-assembled silk fibroin nanofibers for biomedical applications. *Carbohydrate Polymers*,  
602 *251*, 117058.

603 Nie, G., Li, Z., Lu, X., Lei, J., Zhang, C., & Wang, C. (2013). Fabrication of polyacrylonitrile/CuS  
604 composite nanofibers and their recycled application in catalysis for dye degradation. *Applied*  
605 *Surface Science*, *284*, 595-600.

606 Nieto, C., Vega, M. A., Enrique, J., Marcelo, G., & Martín Del Valle, E. M. (2019). Size Matters in the  
607 Cytotoxicity of Polydopamine Nanoparticles in Different Types of Tumors. *Cancers*, *11*(11), 1679.

608 Norowski Jr, P. A., Fujiwara, T., Clem, W. C., Adatrow, P. C., Eckstein, E. C., Haggard, W. O., &  
609 Bumgardner, J. D. (2015). Novel naturally crosslinked electrospun nanofibrous chitosan mats for  
610 guided bone regeneration membranes: material characterization and cytocompatibility. *Journal*  
611 *of Tissue Engineering and Regenerative Medicine*, *9*(5), 577-583.

612 Ouerghemmi, S., Degoutin, S., Tabary, N., Cazaux, F., Maton, M., Gaucher, V., Janus, L., Neut, C., Chai,  
613 F., Blanchemain, N., & Martel, B. (2016). Triclosan loaded electrospun nanofibers based on a  
614 cyclodextrin polymer and chitosan polyelectrolyte complex. *International Journal of*  
615 *Pharmaceutics*, *513*(1), 483-495.



616 Pan, P., Chen, X., Metavarayuth, K., Su, J., & Wang, Q. (2018). Self-assembled supramolecular systems  
617 for bone engineering applications. *Current Opinion in Colloid & Interface Science*, 35, 104-111.

618 Pattnaik, S., Nethala, S., Tripathi, A., Saravanan, S., Moorthi, A., & Selvamurugan, N. (2011). Chitosan  
619 scaffolds containing silicon dioxide and zirconia nano particles for bone tissue engineering.  
620 *International Journal of Biological Macromolecules*, 49(5), 1167-1172.

621 Ranganathan, S., Balagangadharan, K., & Selvamurugan, N. (2019). Chitosan and gelatin-based  
622 electrospun fibers for bone tissue engineering. *International Journal of Biological  
623 Macromolecules*, 133, 354-364.

624 Ryu, J., Ku, S. H., Lee, H., & Park, C. B. (2010). Mussel-Inspired Polydopamine Coating as a Universal  
625 Route to Hydroxyapatite Crystallization. *Advanced Functional Materials*, 20(13), 2132-2139.

626 Sainitya, R., Sriram, M., Kalyanaraman, V., Dhivya, S., Saravanan, S., Vairamani, M., Sastry, T. P., &  
627 Selvamurugan, N. (2015). Scaffolds containing chitosan/carboxymethyl cellulose/mesoporous  
628 wollastonite for bone tissue engineering. *International Journal of Biological Macromolecules*, 80,  
629 481-488.

630 Salerno, A., Fernández-Gutiérrez, M., San Román del Barrio, J., & Domingo, C. (2015). Bio-safe  
631 fabrication of PLA scaffolds for bone tissue engineering by combining phase separation, porogen  
632 leaching and scCO<sub>2</sub> drying. *The Journal of Supercritical Fluids*, 97, 238-246.

633 Saravanan, S., Nethala, S., Pattnaik, S., Tripathi, A., Moorthi, A., & Selvamurugan, N. (2011).  
634 Preparation, characterization and antimicrobial activity of a bio-composite scaffold containing  
635 chitosan/nano-hydroxyapatite/nano-silver for bone tissue engineering. *International Journal of  
636 Biological Macromolecules*, 49(2), 188-193.

637 Shahbazarab, Z., Teimouri, A., Chermahini, A. N., & Azadi, M. (2018). Fabrication and characterization  
638 of nanobiocomposite scaffold of zein/chitosan/nanohydroxyapatite prepared by freeze-drying  
639 method for bone tissue engineering. *International Journal of Biological Macromolecules*, 108,  
640 1017-1027.

641 Shalumon, K. T., Sowmya, S., Sathish, D., Chennazhi, K. P., Nair, S. V., & Jayakumar, R. (2013). Effect  
642 of incorporation of nanoscale bioactive glass and hydroxyapatite in PCL/chitosan nanofibers for  
643 bone and periodontal tissue engineering. *J Biomed Nanotechnol*, 9(3), 430-440.

644 Sharifi, F., Atyabi, S. M., Norouzi, D., Zandi, M., Irani, S., & Bakhshi, H. (2018).  
645 Polycaprolactone/carboxymethyl chitosan nanofibrous scaffolds for bone tissue engineering  
646 application. *International Journal of Biological Macromolecules*, 115, 243-248.

647 Shin, Y. M., Jun, I., Lim, Y.-M., Rhim, T., & Shin, H. (2013). Bio-inspired Immobilization of Cell-Adhesive  
648 Ligands on Electrospun Nanofibrous Patches for Cell Delivery. *Macromolecular Materials and  
649 Engineering*, 298(5), 555-564.

650 Sobocinski, J., Laure, W., Taha, M., Courcot, E., Chai, F., Simon, N., Addad, A., Martel, B., Haulon, S.,  
651 Woisel, P., Blanchemain, N., & Lyskawa, J. (2014). Mussel Inspired Coating of a Biocompatible  
652 Cyclodextrin Based Polymer onto CoCr Vascular Stents. *ACS Applied Materials & Interfaces*, 6(5),  
653 3575-3586.

654 Tsai, W.-B., Chen, W.-T., Chien, H.-W., Kuo, W.-H., & Wang, M.-J. (2013). Poly(dopamine) coating to  
655 biodegradable polymers for bone tissue engineering. *Journal of Biomaterials Applications*, 28(6),  
656 837-848.

657 Van Hong Thien, D., Hsiao, S. W., Ho, M. H., Li, C. H., & Shih, J. L. (2013). Electrospun  
658 chitosan/hydroxyapatite nanofibers for bone tissue engineering. *Journal of Materials Science*,  
659 48(4), 1640-1645.

660 Wen, P., Zong, M.-H., Linhardt, R. J., Feng, K., & Wu, H. (2017). Electrospinning: A novel nano-  
661 encapsulation approach for bioactive compounds. *Trends in Food Science & Technology*, 70, 56-  
662 68.

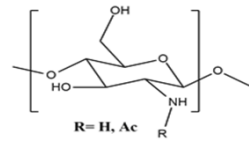
663 Yang, X., Chen, X., & Wang, H. (2009). Acceleration of Osteogenic Differentiation of Preosteoblastic  
664 Cells by Chitosan Containing Nanofibrous Scaffolds. *Biomacromolecules*, 10(10), 2772-2778.

665 Zangmeister, R. A., Morris, T. A., & Tarlov, M. J. (2013). Characterization of Polydopamine Thin Films  
666 Deposited at Short Times by Autoxidation of Dopamine. *Langmuir*, 29(27), 8619-8628.

667 Zia, Q., Tabassum, M., Meng, J., Xin, Z., Gong, H., & Li, J. (2021). Polydopamine-assisted grafting of  
668 chitosan on porous poly (L-lactic acid) electrospun membranes for adsorption of heavy metal  
669 ions. *International Journal of Biological Macromolecules*, 167, 1479-1490.

670

671



**Chitosan**



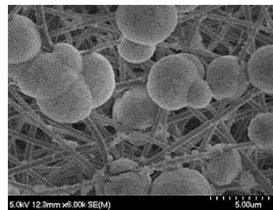
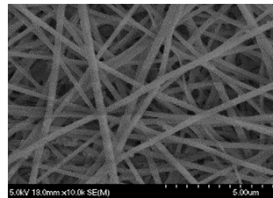
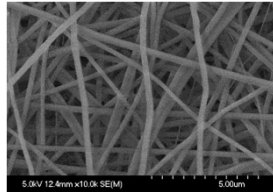
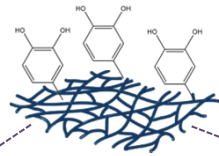
**Electrospinning  
thermal treatment**



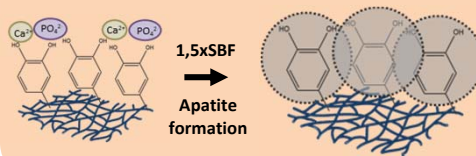
**Nanofibrous scaffold**



**polydopamine**



**In vitro biomineralization**



**Scaffold with osteoconductive  
properties  
for bone reconstruction**